Equation of state of the postperovskite phase synthesized from a natural $(Mg,Fe)SiO_3$ orthopyroxene

Sean R. Shieh*†, Thomas S. Duffy‡, Atsushi Kubo‡, Guoyin Shen§¶, Vitali B. Prakapenka§, Nagayoshi Sata‖, Kei Hirose**, and Yasuo Ohishi††

*Department of Earth Sciences, National Cheng Kung University, Tainan 701, Taiwan; ‡Department of Geosciences, Princeton University, Princeton, NJ 08544; §GeoSoilEnviroCARS, University of Chicago, Chicago, IL 60637; ‖Institute for Research on Earth Evolution, Japan Agency for Marine-Earth Science and Technology, 2-15 Natsushima-Cho, Yokosuka-city, Kanagawa 237-0061, Japan; **Department of Earth and Planetary Sciences, Tokyo Institute of Technology, Tokyo 152-8550, Japan; and ††Japan Synchrotron Radiation Research Institute, 1-1-1 Kouto Sayo-cho, Sayo-gun Hyogo 679-5198, Japan

Edited by Ho-kwang Mao, Carnegie Institution of Washington, Washington, DC, and approved December 22, 2005 (received for review August 7, 2005)

Using the laser-heated diamond anvil cell, we investigate the stability and equation of state of the postperovskite (ppv, $CaIrO_3$-type) phase synthesized from a natural pyroxene composition with 9 mol.% $FeSiO_3$. Our measured pressure-volume data from 12–106 GPa for the ppv phase yield a bulk modulus of 219(5) GPa and a zero-pressure volume of 164.9(6) Å^3 when $K_0' = 4$. The bulk modulus of ppv is 575(15) GPa at a pressure of 100 GPa. The transition pressure is lowered by the presence of Fe. Our x-ray diffraction data indicate the ppv phase can be formed at $P > 109(4)$ GPa and 2,400(400) K, corresponding to ≈400–550 km above the core-mantle boundary. Direct comparison of volumes of coexisting perovskite and $CaIrO_3$-type phases at 80–106 GPa demonstrates that the ppv phase has a smaller volume than perovskite by 1.1(2)%. Using measured volumes together with the bulk modulus calculated from equation of state fits, we find that the bulk sound velocity decreases by 2.3(2.1)% across this transition at 120 GPa. Upon decompression without further heating, it was found that the ppv phase could still be observed at pressures as low at 12 GPa, and evidence for at least partial persistence to ambient conditions is also reported.

phase transition | x-ray diffraction | high pressure | diamond anvil cell | lower mantle

The D″ region of the Earth's mantle lying just above the core-mantle boundary has long been among the least-understood regions of the planet. Seismic studies show D″ to be complex and laterally heterogeneous, including evidence for a D″ seismic discontinuity, anomalous seismic anisotropy, and ultra-low velocity zones (1–3). The ferromagnesian silicate perovskite (pv) phase, $(Mg,Fe)SiO_3$, has been regarded as the dominant lower mantle mineral but its properties are not consistent with those of the D″ region. Thus, the discovery of a postperovskite (ppv) phase at 125 GPa and 2,500 K (4) has attracted considerable attention because of its potential relevance to D″. First-principles quantum mechanical calculations (5–9) support the thermodynamic stability of the new phase and place constraints on some physical properties including the elastic tensor and the Clapeyron slope of the transition. However, theoretical studies involve varying degrees of approximation and thus comparison with direct experiment is essential. Experimental studies have placed constraints on the transition pressure and unit cell parameters of the ppv phase (4, 5, 10–16). Besides the crystal structure, the equation of state (EOS) is the most fundamental parameter obtained from high-pressure experiments. As yet, there has been no experimental study that directly compares the EOSs of the pv and ppv phases over a broad range of pressure conditions for a mantle-relevant chemical composition.

Results and Discussion

Pv and ppv phases were synthesized from an orthopyroxene sample containing 9 mol.% Fe by using the laser-heated diamond anvil cell (see *Experimental Methods*). By using synchrotron x-ray diffraction, we obtained pressure-volume data at 300 K by gradual decompression of the sample without any additional heating. During decompression, the pressure-load relationship of a diamond cell is highly nonlinear, making it very challenging to control the distribution of pressure-volume states achieved. Nevertheless, we were able to successfully measure several data points at very low pressures. The samples were not heated during decompression to avoid back transformation of the metastable ppv phase. Some broadening of diffraction peaks is observed upon decompression. However, argon, which was used as a pressure-transmitting medium, is relatively soft and is expected to limit the level of nonhydrostatic stresses developed. Furthermore, pv and ppv coexist in our samples and thus are subjected to the same stress conditions. The agreement of our pv measurements with earlier data (17–19) as discussed below supports the validity of our results for both the pv and ppv phases.

For the ppv phase, 022 and 131 diffraction lines yielded the strongest intensities. Unit cell parameters were generally refined from these two lines together with 020, 132, and 113. In many cases, 110, 042, and 004 were also used. A representative diffraction pattern is shown in Fig. 1. At pressures <32 GPa, the diffraction intensity of the ppv-phase peaks declined markedly. At these pressures, only 020, 022, 132, and 113 were used for unit cell parameter refinement. For the pv phase, we generally used 101, 110, 111, and 112 for unit cell parameter refinement, although other peaks were included when they could be observed with sufficient intensity. Diffraction peaks were fitted to pseudo-Voigt profile functions and lattice constants at each pressure were determined by least-squares fit. Maximum deviations between measured and calculated unit cell parameters for the ppv phase are 0.2–0.4%. Fig. 2 shows the axial ratios, b/a and c/a, for the ppv phase as a function of pressure (see *Inset*). Although the b/a ratio is larger, both parameters show weak pressure dependence at very high pressures. The results agree well with theoretical predications (5, 6) and available experiments (4, 10, 12, 13).

Fitting the pressure-volume data for the ppv phase to a Birch-Murnaghan EOS (20) yields a bulk modulus, K_0, of 219(5) GPa and an ambient pressure volume, V_0, of 164.9(6) Å^3 for a

Conflict of interest statement: No conflicts declared.

This paper was submitted directly (Track II) to the PNAS office.

Freely available online through the PNAS open access option.

Abbreviations: EOS, equation of state; pv, perovskite; ppv, postperovskite.

†To whom correspondence should be sent at the present address: Department of Earth Sciences, University of Western Ontario, London, ON, Canada N6A 5B7. E-mail: sshieh@uwo.ca.

¶Present address: High Pressure Collaborative Access Team, Advanced Photon Source, Argonne National Laboratory, Argonne, IL 60439.

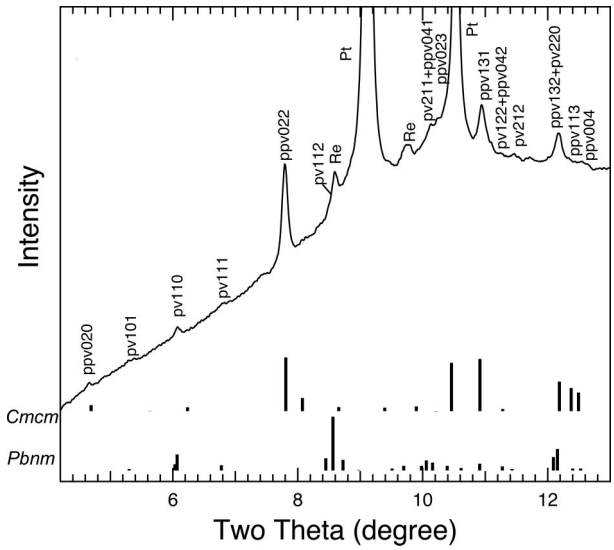

Fig. 1. Integrated x-ray diffraction pattern at 106(2) GPa after quenching from 1,800 K. The unit cell parameters for the ppv phase obtained by least-squares fitting are a = 2.478(7) Å, b = 8.198(23) Å, and c = 6.132(10) Å. Pt, platinum; Re, rhenium. Re peaks are caused by low-intensity tails of the x-ray beam that are incompletely removed by a secondary pinhole system (31). Vertical bars show expected peak positions and relative intensities for pv (*Pbnm*) and ppv (*Cmcm*) phase.

bulk modulus pressure derivative, K_0', fixed at 4 (Fig. 2). The numbers in parentheses represent 1-σ uncertainties. Our results are compared with theoretical studies for $MgSiO_3$ ppv and experimental studies for $MgSiO_3$ pv phase in Table 1. To illustrate the tradeoffs, if we fix $K_0' = 4.4$, we obtain $V_0 = 166.2(7)$ Å^3 and $K_0 = 198(5)$ GPa, which are close to generalized gradient approximation results from Oganov and Ono (5) (Table 1). On the whole, the good agreement between theory and experiment indicates that low concentrations of Fe do not strongly affect the bulk modulus of the ppv phase (Table 1). Our measured unit cell volumes of the ppv phase at $P > 100$ GPa are also consistent with experimental data reported on both Fe-free and Fe-bearing samples (4, 5, 10, 12, 13) (Fig. 2). The EOS for pv was calculated by using pressure-volume data at 83–106 GPa together with the experimentally determined zero-pressure volume from the recovered sample [V_0 = 163.3(1) Å^3], which is consistent with the expected value for Fe-free and Fe-bearing pv (17, 18). The resulting EOS parameters are compared with previous experiments in Table 1. The measured unit cell volumes of the pv phase are consistent with previous studies (17, 18) (Fig. 2).

Because of the relative paucity of low-pressure data and long extrapolation from the stability field of the ppv phase, our zero-pressure EOS parameters necessarily suffer from some uncertainty. Therefore, in this study we specifically aimed to obtain coexistence of pv and ppv rather than a single phase of either. This approach allows direct comparison of the volumes and bulk moduli of the two phases at deep lower mantle pressures. It is especially challenging to obtain good-quality diffraction patterns in this case because synthesis must be performed near the phase boundary where kinetics are very sluggish. Diffraction intensities are reduced because the amount of each phase is smaller and there are also peak overlaps. However, the advantage of our approach is that we are making a direct comparison of properties of the two phases under identical experimental conditions that are not subject to errors caused by pressure and stress state variations between samples.

A direct comparison of the volumes of pv and ppv at 83–106 GPa shows that the ppv phase has 1.1(2)% lower volume than the pv phase. For comparison, theoretical studies (5–6, 8) of the Fe-free end member have estimated volume changes of 1.4–1.6% at 120 GPa, somewhat larger than our experimental results. By differentiating the pressure-volume EOS, the bulk moduli of both phases were computed as a function of pressure. The bulk modulus of the ppv phase is 575(15) GPa at 100 GPa pressure and 641(17) GPa at 120 GPa. First-principles static calculations yield similar values of 647–681 GPa at the latter pressure (5–9). Our calculated bulk modulus for pv at 120 GPa is 663(26) GPa.

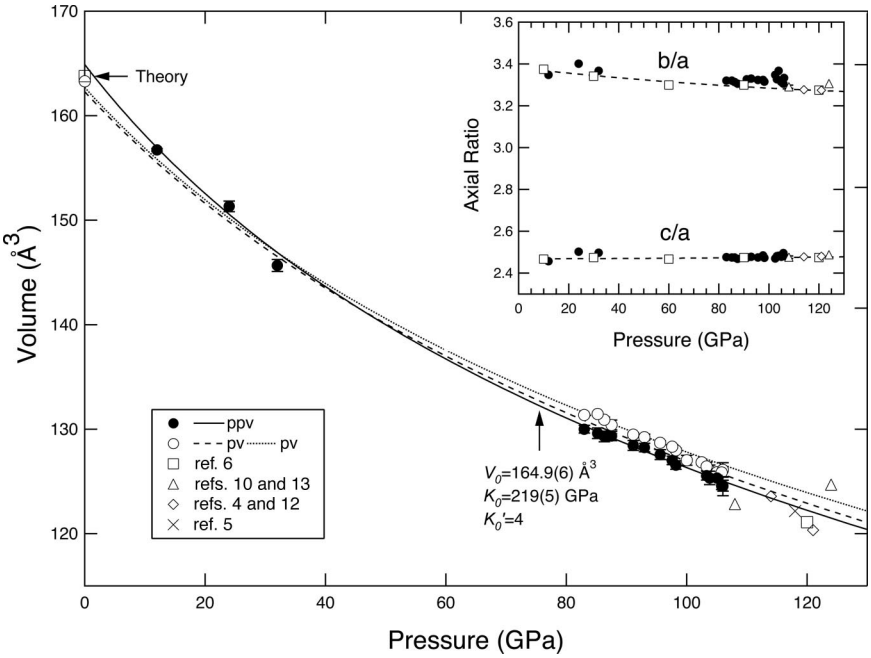

Fig. 2. The EOS of pv and ppv phases. The dashed and dotted curves are the experimentally determined EOS for $MgSiO_3$ pv (17) and $Mg_{0.95}Fe_{0.05}SiO_3$ pv (18), respectively. The solid curve shows a second-order Eulerian finite strain fit ($K_0' = 4.0$) to the ppv-phase data. The theoretical zero-pressure volume for ppv is from Tsuchiya *et al.* (6). (*Inset*) The pressure dependence of the axial ratios of the ppv phase.

Table 1. Comparison of EOS parameters of ppv and pv phases obtained from this study and previous work

	$CaIrO_3$-type				pv			
Parameter	Ref. 5, LDA	Ref. 5, GGA	Ref. 24, LDA	This study, experiment	Ref. 17, experiment	Ref. 18, experiment	Ref. 19, experiment	This study, experiment
V_0 (Å^3)	162.9	167.6	163.8	164.9 (6)	162.3	162.7	—	163.3 (1)
K_0 (GPa)	231.9	200.0	215.9	219 (5)	259 (1)	255.4	253 (3)	255 (10)
dK_0/dP	4.4	4.5	4.41	4.0*	3.7 (4)	4.0*	—	3.7*

LDA, local density approximation; GGA, generalized gradient approximation.
*Fixed value.

Thus, the bulk moduli of pv and ppv overlap within mutual uncertainties. Again, this finding is consistent with theoretical calculations (5–9). Despite being the high-pressure phase, it is possible that ppv has a lower bulk modulus than pv at deep mantle pressures. Reduction in bulk modulus across high-pressure phase transitions has been observed in a number of oxide systems in which there are additional compression mechanisms available in the high-pressure phase (21). The enhanced compressibility along the *b*-axis may be responsible for this effect in the ppv phase. Combining the results for volume and bulk modulus indicates that at 120 GPa the bulk sound velocity changes by −2.3(2.1)% across the transition at deep mantle pressures. Theoretical studies have predicted that the decrease in bulk sound velocity will be <1% across the transition (5, 8). Our results are consistent with those studies, but also allow for a greater decrease in bulk sound velocity up to ≈4%.

At low pressures, the volume of ppv apparently becomes greater than that of pv (17, 18) (Fig. 2). Unfortunately, the diffraction patterns of pv become sufficiently weak at these low pressures such that a reliable volume cannot be obtained from our experiments. In this case, because of the paucity of low-pressure data and the possible effects of deviatoric stress in comparing our results on ppv with the pv EOS (17, 18), further experiments will be necessary to determine volume relationships between the two phases in the low-pressure metastable region.

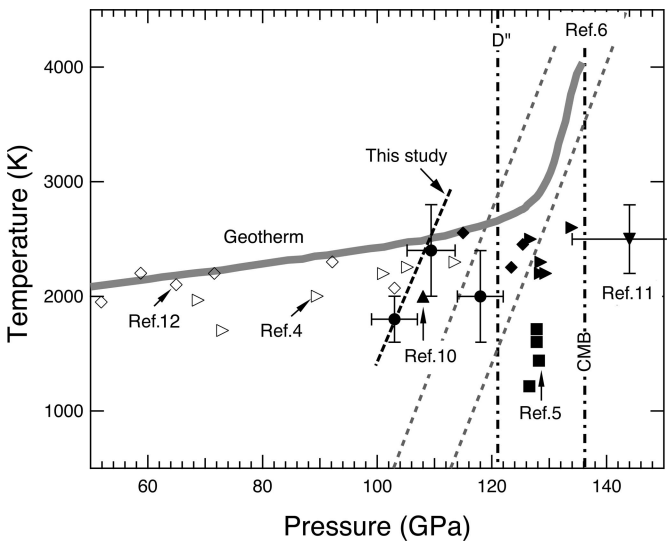

Fig. 3. Phase diagram for the (Mg,Fe)SiO_3 system obtained from both experiment and theory. Pressure-temperature conditions at which ppv phase was observed (together with pv phase) in the present study are indicated by ●. For other studies, diamonds and upward-pointing triangles are for Fe-bearing samples, other symbols are for Fe-free samples. Filled symbols, ppv; open symbols, pv. Theoretical bounds on Clapeyron slope of ppv-phase transition in $MgSiO_3$ (dashed light lines) are from Tsuchiya *et al.* (6). The dashed dark line is drawn through the present data with the same slope. The geotherm is from ref. 32. CMB, core-mantle boundary.

Our results indicate the ppv phase can be synthesized at 109(4) GPa and 2,400(400) K for a starting sample with 9 mol.% $FeSiO_3$ (Fig. 3). This result is in agreement with other experiments (10, 12). Along an estimated mantle geotherm the transition would occur ≈400–550 km above the core-mantle boundary (Fig. 3). Conversely, to ascribe the ppv transition to the D″ discontinuity (1, 2) would require temperatures of ≈3,500–4,000 K in the deep lower mantle. However, there are a number of complicating factors, including multicomponent chemical effects, pressure scale uncertainties (22), Clapeyron slope uncertainties, and the effects of the transformation itself on mantle dynamics and the geotherm (23), that must be considered in drawing conclusions about the phase boundary. The sluggish kinetics of the transformation indicates that our measured pressure is an upper bound to the transition pressure, however.

Upon reduction of pressure <30 GPa, the diffraction lines of the ppv phase weaken but were still clearly observable at 24 and 12 GPa. The strongest diffraction line of the ppv phase 022 could even be observed after the sample was returned to ambient pressure and temperature conditions (Figs. 4 and 5). The measured *d*-spacing of the 022 ppv peak was 2.688 Å comparable with the theoretically calculated value of 2.690 Å (J. Tsuchiya, personal communication). The weakening and loss of most diffraction peaks except 022 suggests possible partial amorphization of the sample. Indeed, the 022 peak was still detectable but considerably less intense when the sample was examined again 7 days after it was first quenched. The presence of relatively low levels of deviatoric stresses through the use of an Ar pressure medium in this study might enhance the stability of the $CaIrO_3$-type phase at ambient conditions compared with other studies that have used harder pressure media. Our observation of metastability of the ppv phase at low and even ambient pressures is consistent with theoretical predictions (24). However, in other experimental studies the ppv phase was found to be amorphous when examined by transmission electron microscopy upon recovery to ambient pressure but no information was provided on the stability of the ppv phase at low pressure (≈10 GPa) (12, 14). The ppv phase of $MgGeO_3$ has been reported to remain metastable upon decompression to 6 GPa (25).

Experimental Methods

The composition of the natural orthopyroxene as determined by electron microprobe analysis was $(Mg_{1.80}Fe_{0.18}Al_{0.01}Ca_{0.01})Si_2O_6$. Powder x-ray diffraction confirmed the sample to be pure orthopyroxene with a_0 = 18.244 Å, b_0 = 8.837 Å, c_0 = 5.186 Å, and V_0 = 836.07 Å^3. The samples were loaded into a 50-μm diameter rhenium gasket hole of a diamond anvil cell. The rhenium gaskets were 25–27 μm in thickness after preindentation. Samples were compressed by using a symmetric diamond cell with 150-μm-diameter beveled culets. Pt, Au, or NaCl were used as internal pressure standards (26–28). Ar and NaCl were used as insulation and pressure transmitting media.

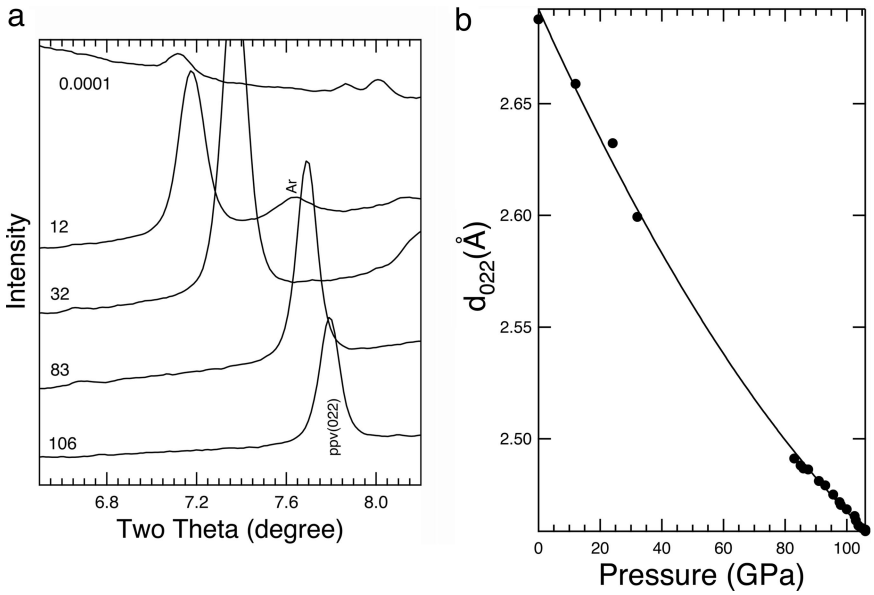

Fig. 4. The evolution of ppv diffraction peak 022 during decompression. (*a*) The pressure (in GPa) is shown next to each spectrum. Ar denotes argon diffraction peak. Intensities at different pressures are relative as samples are textured, and in some cases integration was over full diffraction rings and over partial rings in other cases. (*b*) The solid curve shows a polynomial fit to the measured *d*-spacings for the $CaIrO_3$-type 022 peak (●).

High-pressure x-ray diffraction experiments were performed at beamline 13-ID-D of the GeoSoilEnviroCARS sector of the Advanced Photon Source and at BL10XU of SPring-8 (Japan Synchrotron Radiation Research Institute). At GeoSoilEnviroCARS, a monochromatic x-ray beam with a wavelength of 0.3344 Å was focused to 5-by-6 μm^2 by a pair of Kirkpatrick-Baez mirrors. The x-ray diffraction patterns were collected by a MAR345 image plate with exposure times of 60 or 180 s. Two-dimensional diffraction images were analyzed by using the program FIT2D (29). CeO_2 was used as a standard to determine the distance and orientation of the detector. Integrated one-dimensional diffraction patterns were obtained from full rings but also in some cases by restricting integrations to partial rings, to enhance signal in textured patterns. Samples were heated by using the double-sided laser heating system at GeoSoilEnviroCARS (30, 31). A TEM_{00} (transverse electromagnetic mode) Nd:YLF laser with a hotspot of ≈20-μm diameter was used to achieve temperatures of ≈1,700–1,880 K for heating times of 30–36 min.

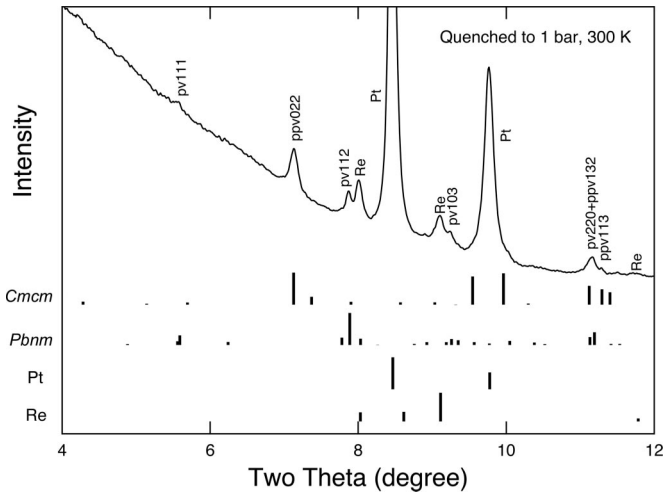

Fig. 5. Integrated x-ray diffraction pattern for the recovered sample. The two-dimensional image is highly textured as reflected by the prominent 022 diffraction peak for the ppv phase, whereas other ppv peaks are weak (ppv113) and/or overlapped (ppv 131). The abbreviations are the same as in Fig. 1.

At BL10XU, a monochromatic beam, with wavelength of either 0.4129 or 0.4150 Å, was collimated to 20-μm diameter and directed through the diamond anvil cell. The x-ray diffraction patterns were recorded by a Rigaku (Tokyo) image plate with exposure times from 180 to 300 s. The samples were also heated by a multimode Nd:YAG or a TEM_{01} (transverse electromagnetic mode) Nd:YLF laser, using doubled-sided heating. The heating spot was >20 μm, and temperatures ranged from 2,000 to 2,400 K.

Experiments using three different sample configurations were conducted. For the first experiment (carried out at the Advanced Photon Source), the sample mixed with 10 wt.% Pt, which served as a pressure medium and laser absorber. Argon was loaded cryogenically to thermally insulate the sample from the diamond anvils. The sample was compressed directly to 106(2) GPa. Before heating, weak and broad diffraction peaks were observed, implying a disordered or partially amorphous sample material after cold compression. The sample was then heated to 1,880(50) K for 36 min. After temperature quenching, the ppv ($CaIrO_3$-type) and pv phases were observed to coexist. The pressure after heating was 100(1) GPa. The sample was then compressed to 106 GPa, and several additional heating cycles (for ≈90 min total) were conducted at 1,700–1,800 K. The coexistence of pv and $CaIrO_3$-type peaks continued to be observed with no significant change in their relative intensities, which indicates that once converted to the pv phase, the transition to the ppv phase proceeds much more slowly than that from initially disordered or amorphous material.

In the second experiment (SPring-8), an orthopyroxene plus Au mixture was directly compressed to 105 GPa and heated for 30 min. NaCl was used as an insulating medium. *In situ* x-ray diffraction patterns showed peaks assignable to both the pv and ppv phases at 109(4) GPa and 2,400(400) K. In the third experiment (SPring-8), an orthopyroxene sample was insulated from the diamonds by using NaCl layers, which also served as the pressure standard. The sample was directly compressed to 115(5) GPa and heated to 2,000(400) K for ≈30 min. Again, the pv and ppv phases were observed to coexist, and they continued to be observed after ≈60 min of additional

heating. Limitations in available beam time prevented decompression experiments from being conducted for the samples synthesized at SPring-8, and these data are mainly used to establish the pressure-temperature conditions at which the ppv phase can be observed for this composition.

We thank Y. Iizuka for the microprobe data analysis and the reviewers and editor for their comments that improved the manuscript. This work was supported by the National Science Foundation, the Packard Foundation, the National Science Council, and the National Synchrotron Radiation Research Center. Portions of this work were performed at GeoSoilEnviroCARS, Advanced Photon Source, Argonne National Laboratory. GeoSoilEnviroCARS is supported by the National Science Foundation, the Department of Energy, and the state of Illinois. Use of the Advanced Photon Source was supported by the Department of Energy Basic Energy Sciences.

1. Wysession, M. E., Lay, T., Revenaugh, J., Williams, Q., Garnero, E., Jeanloz, R. & Kellog L. (1998) in *The Core-Mantle Boundary Region*, eds. Gurnis, M., Wysession, M. E., Knittle E. & Buffet, B. A. (American Geophysical Union, Washington, DC), Vol. 28, pp. 273–297.
2. Sidorin, I., Gurnis, M. & Helmberger, D. V. (1999) *Science* **286,** 1326–1331.
3. Garnero, E. J. (2000) *Annu. Rev. Earth Planet. Sci.* **28,** 509–537.
4. Murakami, M., Hirose, K., Kawamura, K., Sata, N. & Ohishi, Y. (2004) *Science* **304,** 855–858.
5. Oganov, A. R. & Ono, S. (2004) *Nature* **430,** 445–448.
6. Tsuchiya, T., Tsuchiya, J., Umemoto, K. & Wentzcovitch, R. M. (2004) *Earth Planet. Sci. Lett.* **224,** 241–248.
7. Tsuchiya, T., Tsuchiya, J., Umemoto, K. & Wentzcovitch, R. M. (2004) *Geophys. Res. Lett.* **31,** L14603.
8. Iitaka, T., Hirose, K., Kawamura, K. & Murakami, M. (2004) *Nature* **430,** 442–445.
9. Stackhouse, S., Brodholt, J. P., Wookey, J., Kendall, J. M. & Price, G. D. (2005) *Earth Planet. Sci. Lett.* **230,** 1–10.
10. Mao, W. L., Shen, G., Prakapenka, V. B., Meng, Y., Cambell, A. J., Heinz, D. L., Shu, J., Hemley, R. J. & Mao, H. K. (2004) *Proc. Natl. Acad. Sci. USA* **101,** 15867–15869.
11. Shim, S.-H., Duffy, T. S., Jeanloz, R. & Shen, G. (2004) *Geophys. Res. Lett.* **31,** L10603.
12. Murakami, M., Hirose, K., Sata, N. & Ohishi, Y. (2005) *Geophys. Res. Lett.* **32,** L03304.
13. Mao, W. L., Meng, Y., Shen, G., Prakapenka, V. B., Campbell, A. J., Heinz, D. L., Shu, J., Caracas, R., Cohen, R. E., Fei, Y. *et al.* (2005) *Proc. Natl. Acad. Sci. USA* **102,** 9751–9753.
14. Kobayashi, Y., Kondo, T., Ohtani, E., Hirao, N., Miyajima, N., Yagi, T., Nagase, T. & Kikegawa, T. (2005) *Geophys. Res. Lett.* **32,** L19301.
15. Ono, S. & Oganov, A. R. (2005) *Earth Planet. Sci. Lett.* **236,** 914–932.
16. Hirose, K, Takafuji, N., Sata, N. & Ohishi, Y. (2005) *Earth Planet. Sci. Lett.* **237,** 239–251.
17. Fiquet, G., Dewale, A., Andrault, D., Kunz, M. & Le Bihan, T. (2000) *Geophys. Res. Lett.* **27,** 21–24.
18. Andrault, D., Bolfan-Casanova, N. & Guignot, N. (2001) *Earth Planet. Sci. Lett.* **193,** 501–508.
19. Sinogeikin, S. V., Zhang, J. & Bass, J. D. (2004) *Geophys. Res. Lett.* **31,** L06620.
20. Poirier, J. P. (2000) *Introduction to the Physics of the Earth's Interior* (Cambridge Univ. Press, Cambridge, U.K.).
21. Haines, J., Leger, J. M. & Schulte, O. (1996) *J. Phys. Condens. Matt.* **8,** 1631–1646.
22. Hirose, K., Sinmyo, R., Sata, N. & Ohishi, Y. (2006) *Geophys. Res. Lett.* **33,** L01310.
23. Nakagawa, T. & Tackley, P. J. (2004) *Geophys. Res. Lett.* **31,** L16611.
24. Tsuchiya, J., Tsuchiya, T. & Wentzcovitch, R. M. (2005) *J. Geophys. Res.* **110,** B02204.
25. Hirose, K., Kawamura, K., Ohishi, Y., Tateno, S. & Sata, N. (2005) *Am. Mineral.* **90,** 262–265.
26. Holmes, N. C., Moriarty, J. A., Gather, G. R. & Nellis, W. J. (1989) *J. Appl. Phys.* **66,** 2962–2967.
27. Shim, S.-H., Duffy, T. S. & Takemura, K. (2002) *Earth Planet. Sci. Lett.* **203,** 729–739.
28. Sata, N., Shen, G., Rivers, M. L. & Sutton, S. R. (2002) *Phys. Rev. B* **65,** 104114.
29. Hammersley, A. P., Svensson, S. O., Hanfland, M., Fitch, A. N. & Hausermann, D. (1996) *High Press. Res.* **14,** 235–248.
30. Shen, G., Rivers, M. L., Wang, Y. & Sutto, S. R. (2001) *Rev. Sci. Instru.* **72,** 1273–1282.
31. Shen, G., Prakapenka, V. B., Eng, P. J., Rivers, M. L. & Sutton, S. R. (2005) *J. Synchrotron Rad.* **12,** 642–649.
32. Boehler, R. (2000) *Rev. Geophys.* **38,** 221–246.